MOL #93450

1. Title page

Label-Free Monitoring of Mu Opioid Receptor-Mediated Signaling

Philippe Bourassa, Hanieh Bagheri Tudashki, Graciela Pineyro, Michel Grandbois and Louis Gendron

Département de physiologie et biophysique (P.B., L.G.)

Département de pharmacologie (H.B.T., M.G.)

Département de psychiatrie (G.P.)

Centre de recherche du CHU Ste-Justine, Université de Montréal (H.B.T, G.P.)

Institut de pharmacologie de Sherbrooke (M.G., L.G.)

Centre de recherche clinique Étienne-Le Bel (M.G., L.G.)

Université de Sherbrooke, Sherbrooke, Québec, Canada (P.B., M.G., L.G.)

Quebec Pain Research Network (L.G.)

1

MOL #93450

2. Running title page

a) **Running title**: Surface Plasmon Resonance to Assess Signaling Cascades

b) **Correspondence**: Louis Gendron, Ph.D.
Département de physiologie et biophysique
Université de Sherbrooke
Faculté de médecine et des sciences de la santé
Sherbrooke, Quebec, Canada
Tel: (819) 820-6868 ext 12760, Fax: (819) 820-6887
Email: Louis.Gendron@USherbrooke.ca

Michel Grandbois, Ph.D.
Département de pharmacologie
Université de Sherbrooke
Faculté de médecine et des sciences de la santé
Sherbrooke, Quebec, Canada
Tel: (819) 820-6868 ext 12369, Fax: (819) 564-5400
Email: Michel.Grandbois@USherbrooke.ca

c)
Text pages: 39

Tables: 2

Figures: 10

References: 42

Abstract: 231 words

Introduction: 538 words

Discussion: 1614 words

d) BRET, bioluminescence resonance energy transfer; CTAP, D-Phe-Cys-Tyr-D-Trp-Arg-Thr-Pen-Thr-NH2; CTOP, D-Phe-Cys-Tyr-D-Trp-Orn-Thr-Pen-Thr-NH2; CTX, cholera toxin; DAMGO, Tyr-D-Ala-Gly-N-methyl-Phe-Gly-ol; Dynasore, 3-Hydroxynaphthalene-2-carboxylic acid-(3,4-dihydroxybenzylidene)-hydrazide; ERK1/2, extracellular signal-regulated kinases; GPCR, G protein-coupled receptor; GTPγS, guanosine 5'-O-(3-thiotriphosphate); MOP, mu opioid receptor; PTX, pertussis toxin; SPR, surface plasmon resonance; U0126, 1,4-Diamino-2,3-dicyano-1,4-*bis*(2-aminophenylthio)butadiene.

3. Abstract

In this study, we used a combination of traditional signaling investigation approaches, bioluminescence resonance energy transfer (BRET) biosensors and the label-free approach Surface Plasmon Resonance (SPR) spectroscopy to monitor the signaling cascades of the mu opioid receptor (MOP). In HEK cells stably expressing a Flag-tagged version of human MOP, we compared the signals triggered by the non-internalizing and internalizing MOP agonists morphine and DAMGO, respectively. We studied three major and well-described components of MOP signaling: receptor internalization, G protein coupling, and ERK1/2 activation. Our results show that morphine and DAMGO display different profiles of receptor internalization and a similar ability to trigger the phosphorylation of ERK1/2. Our SPR analyses revealed that morphine and DAMGO evoke similar SPR signatures and that $G\alpha_i$, cAMP-dependent pathways, and ERK1/2 have key roles in morphine- and DAMGO-mediated signaling. Most interestingly, we found that the so-called MOP neutral antagonists CTOP, naloxone, and naltrexone behave like partial agonists. Even more intriguing, BRET experiments indicate that CTAP induces similar conformational changes as naltrexone at the $G\alpha_i$-$\beta\gamma$ interface whereas it appears as an inverse agonist based on its SPR response thus indicating distinct signaling mechanisms for the two ligands. Taken altogether, our results support the usefulness of label-free methods such as SPR to study whole-cell responses and signaling cascades triggered by G protein-coupled receptors (GPCRs) and complement the conventional approaches by revealing cellular responses that would have been undetectable otherwise.

MOL #93450

4. Introduction

Opioids targeting the mu opioid receptors (MOPs) are still the most powerful analgesics used for the treatment of moderate to severe pain conditions (Melnikova, 2010). However, the use of MOP agonists is often limited by the occurrence of adverse effects, such as constipation and nausea (Cherny et al., 2001). As a member of the class A G protein-coupled receptors (GPCRs), MOP is coupled to the heterotrimeric G protein $G\alpha_i$, which leads to the inhibition of the adenylyl cyclase and a decrease in cAMP levels. Additionally, the activation of MOP leads to the inhibition of voltage-gated calcium channels and the activation of G protein-coupled inwardly rectifying potassium channels (GIRK) (Williams et al., 2001). Several differences have been noted among MOP agonists with regard to the signaling pathways they trigger (Arttamangkul et al., 2008; Zheng et al., 2008; McPherson et al., 2010), which is consistent with the concept of functional selectivity in which different ligands targeting the same receptor can elicit distinct signaling cascades (Urban et al., 2007). In this context, the molecular events specifically leading to analgesia and adverse effects have not been thoroughly described. Consequently, a better understanding of these events is required for the development of new opioid drugs with reduced adverse effects (Raehal et al., 2011).

The assessment of functional selectivity requires the evaluation of global cell responses following the activation of a GPCR. Therefore, a valuable approach to study this phenomenon would be to use a technology capable of detecting any change within the cell induced by the activation of a receptor. Whole cell biosensors such as impedance- and optical-based detection systems may serve this need (Ciambrone et al., 2004; Cunningham et al., 2004; Fang et al., 2006). Compared with traditional assays, whole cell

biosensors offer the possibility to globally evaluate multiple aspects of the cell response in a single, highly sensitive assay (Giaever and Keese, 1993; Scott and Peters, 2010). These approaches do not require fluorescent or radioactive probes, which can affect the functions of some proteins within the cell (Cooper, 2006). Recent reports demonstrated the usefulness of whole cell biosensors to study functional selectivity of several GPCRs. As examples, Bouvier's group used an impedance-based system to assess functional selectivity at the β_2 adrenergic receptor (Stallaert et al., 2012), whereas Fang's group used an optical-based system to assess opioid receptor signaling (Morse et al., 2011; Morse et al., 2013). We previously showed that SPR represents a valuable label-free technique to monitor GPCR signaling and apoptosis (Cuerrier et al., 2008; Chabot et al., 2009; Maltais et al., 2012).

In the present study, we use SPR as a sensitive label-free technique to assess functional selectivity of MOP signaling in living cells. We hypothesized that distinct signaling pathways triggered by different ligands acting on the same receptor can be assessed by analyzing distinctive SPR signals. We used DAMGO and morphine as selective MOP agonists because they are known to exhibit distinct signaling properties, and we evaluated the contribution of three different MOP signaling components in the SPR responses, i.e., receptor internalization, G protein coupling, and ERK1/2 activation. We also evaluated the implication of G protein coupling in the SPR responses generated by four MOP ligands previously described as antagonists (Mulder et al., 1991; Janecka et al., 2004).

MOL #93450

5. MATERIALS AND METHODS

Cell Culture

HEK 293 cells stably expressing Flag-tagged human MOP (HEK FlagMOP), with a receptor density of 2.5 pmol/mg of cell proteins (Morse et al., 2011), were kindly provided by Dr. Mark von Zastrow (University of California, San Francisco, CA). The cells were grown at 37°C in Dulbecco Modified Eagle Medium (DMEM) supplemented with 10% heat-inactivated fetal bovine serum and 50 mg/L of gentamicin in a humidified atmosphere of 95% air and 5% CO_2. The cells were maintained in a medium containing 250 µg/mL of the selection agent G418.

MOP internalization assay

HEK FlagMOP cells were grown on poly-L-lysine-coated glass coverslips for 2-3 days until they reached 60-70% confluence. Before stimulation, the cells were starved with DMEM for 30 min with or without 80 µM of dynasore (BioVision Incorporated, Milpitas, CA). The cells were then stimulated with 1 µM DAMGO (Tocris Bioscience, R&D Systems, Minneapolis, MN) or with 1 µM morphine sulfate (Sandoz Canada, Boucherville, Canada). The stimulation was terminated by the aspiration of the culture medium and the addition of ice-cold phosphate-buffered saline (PBS) (140 mM NaCl, 2.7 mM KCl, 8.1 mM Na_2HPO_4 and 1.5 mM KH_2PO_4; pH 7.2). Next, the cells were fixed for 15 min with an ice-cold 4% paraformaldehyde solution in PBS. The cells were washed three times with a 0.02% Triton X-100 solution in PBS (PBST), followed by a 10 min block with a PBST solution containing 2% of bovine serum albumin (PBST/BSA). After

MOL #93450

blocking, the cells were incubated for 2 h at room temperature with a mouse anti-FLAG M1 antibody (1:1000; Sigma-Aldrich, St. Louis, MO) in PBST/BSA supplemented with 1 mM Ca^{2+} (PBST-Ca^{2+}/BSA). Next, the cells were washed three times with the PBST-Ca^{2+} solution, blocked for 5 min in PBST-Ca^{2+}/BSA, and incubated for 1 h at room temperature with Alexa Fluor® 488 goat anti-mouse antibody (1:1000; Life Technologies, Burlington, Canada) in PBST-Ca^{2+}/BSA. Finally, the cells were washed three times with PBST-Ca^{2+}, and the coverslips were mounted on microscope glass slides with AquaPolymount (Polysciences, Warrington, PA). For each condition, 26-30 cells were imaged using a Fluoview 1000 (FV1000) laser scanning confocal IX81 Olympus microscope (Olympus America, Center Valley, PA) equipped with a ProScan II motorized stage system (Prior scientific, Rockland, MA) and fitted with a U plan S-Apo 60X (1.35 NA) oil-immersion objective. Each micrograph represents an optical slice of 0.31 µm and displays a clear horizontal section of the cell nucleus. Pixel quantification was performed using a custom-built software integrated to ImageJ. This software allows for the calculation of intracellular and cell membrane pixels. The membrane thickness was fixed at a width of 6 pixels throughout the analysis of each condition. Pseudo-colors were used to easily distinguish between intracellular (green) and cell membrane (purple) pixels. The results obtained from those analyses were expressed as a ratio of intracellular / cell membrane pixels.

MOL #93450

MOP-induced ERK1/2 activation

HEK FlagMOP cells were starved for 30 min with DMEM and then stimulated for 3 min with increasing concentrations of DAMGO or morphine (10^{-10} to 10^{-7} M for DAMGO and 10^{-9} to 10^{-6} M for morphine). When indicated, various pharmacological inhibitors were used prior to stimulation with DAMGO or morphine to evaluate the contribution of distinct signaling components to the MOP-mediated activation of ERK1/2 (CTAP, a MOP selective antagonist, 10 µM for 30 min; dynasore, a dynamin inhibitor, 80 µM for 30 min; pertussis toxin (PTX), a $G\alpha_i$ protein inhibitor, 100 ng/mL for 20 h; cholera toxin (CTX), a $G\alpha_s$ protein activator, 400 ng/mL for 20 h; U0126, a MEK inhibitor, 0.02 to 20 µM for 30 min). The stimulation was terminated by the aspiration of the culture medium and by the addition of ice-cold Hank's buffered saline (HBS) (130 mM NaCl, 3.5 mM KCl, 1.8 mM $CaCl_2$, 0.5 mM $MgCl_2$, 2.5 mM $NaHCO_3$, 5 mM HEPES and 0.5 mM EGTA). The cells were then stabilized with ice-cold HBS containing 2 mM Na_3VO_4, 0.1 µM staurosporine and Complete™ protease inhibitors (Roche Diagnostics, Indianapolis, IN) for 10 min. Cell lysates were obtained using a 50 mM HEPES pH 7.8 solution containing 1% Triton X-100, 2 mM Na_3VO_4, 0.1 µM staurosporine, and Complete™ protease inhibitors. The lysates were transferred to 1.5-mL Eppendorf tubes and centrifuged for 10 min at 13500 g at 4°C. The supernatants were saved and stored at -20°C until use. The protein extracts (35 µg per sample) were resolved on a 10% SDS-polyacrylamide gel and transferred to polyvinylidene fluoride (PVDF) membranes. The PVDF membranes were then blocked for 1 h using a Tris-buffered saline with 0.05% Tween 20 (TBS-T) containing 1% gelatin. After blocking, the membranes were incubated for 2 h at room temperature with rabbit anti-phospho ERK1/2 or anti-ERK1/2 antibodies

8

MOL #93450

(both 1:1000; Cell Signaling Technology, Danvers, MA). Finally, the PVDF membranes were washed three times with TBS-T and incubated for 1 h at room temperature with a horseradish peroxidase-conjugated (HRP) anti-rabbit antibody (1:2000; GE Healthcare Life Sciences, Piscataway, NJ). Proteins were detected using an enhanced chemiluminescence detection kit (Amersham™ ECL™ Western Blotting Detection Reagents from GE Healthcare Life Sciences). Densitometric analysis was performed with ImageJ, and the results are reported as the fold increase over the control.

Surface Plasmon Resonance measurements

Gold substrates were prepared and Surface Plasmon Resonance (SPR) experiments were conducted as previously described (Cuerrier et al., 2008; Maltais et al., 2012). The HEK FlagMOP cells were grown to confluence on a gold substrate surface pre-coated with a solution of 5 µg/mL fibronectin (Sigma-Aldrich) and 200 µg/mL gelatin (BD, Franklin Lakes, NJ). Prior to stimulation, the cells were starved for 30 min with DMEM and stabilized in a HEPES-buffered salt solution (HBSS, pH 7.4) containing 20 mM HEPES, 120 mM NaCl, 5.3 mM KCl, 1.8 mM $CaCl_2$, 0.8 mM $MgSO_4$ and 11.1 mM dextrose, for 30 min at 37°C. The pharmacological inhibitors presented above were used in SPR experiments to evaluate the contribution of their targeted signaling components in the SPR signatures obtained for DAMGO and morphine. In addition, EGF was used to confirm the viability of the cells following a 20 h incubation in the presence of PTX. SPR data were analyzed with MatLab® R2009a (The MathWorks, Natick, MA) and smoothed using a moving average filter to allow maximal slope evaluation.

MOL #93450

Phase-contrast microscopy

HEK FlagMOP were grown to confluence in 35-mm Petri dishes. Prior to the assay, the cells were starved in DMEM for 30 min and stabilized in HBSS during 30 min. Two minutes of baseline recording were performed before the incubation of the cells with 10 µM of each antagonist. The images were obtained with the 10X objective of an Axio Observer Z1 microscope equipped with an Axio MRm camera (Carl Zeiss Canada, North York, Canada) at intervals of 10 sec for 30 min at 37°C.

BRET experiments

DNA constructs

The plasmid encoding GFP fused at the amino-terminus of human Gγ2 was obtained by subcloning the human Gγ2 coding sequence into GFP vectors (Gales et al., 2005). The recombinant plasmid encoding for human $G\alpha_{i1}$-Luc91 was prepared using a flexible linker to insert the coding sequence of humanized *Renilla* luciferase (*R*Luc; PerkinElmer Life Sciences, Waltham, MA) into that of human $G\alpha_{i1}$ between residues Leu91 and Lys92. Mouse MOP DNA in pCDNA3.1/Zeo was kindly provided by Dr. Alain Beaudet (McGill University, Montreal, Canada).

Cell culture and transfection

For BRET assays, HEK 293 cells were seeded at a density of 3.5×10^6 cells in 100 mm Petri dishes, cultured for 24 h, and transiently transfected with $G\beta_1$ (3 µg), mouse MOP (8 µg), GFP-$G\gamma_2$ (3 µg), and $G\alpha_{i1}$-Luc 91 (0.6 µg) (values for 100 mm Petri dish) using polyethylenimine as indicated by the manufacturer. Experiments were carried out 48 h post-transfection. Cells were grown and maintained in Dulbecco's modified Eagles'

10

medium supplemented with 10% fetal bovine serum, 2 mM L-glutamine, 100 unit/ml penicillin-streptomycin, at 37ºC in humidified atmosphere at 95% air and 5% CO_2 (Audet et al., 2012).

Monitoring conformational changes within the Gαβγ heterotrimer

The way different MOP ligands modified $G\alpha_i$ interaction with the Gβγ dimer was assessed using a methodology that we had previously developed and validated for detection of ligand-induced conformational changes within GPCR signaling complexes (Audet et al., 2008; Audet et al., 2012). Forty-eight hours after transfection, cells were washed twice and mechanically detached at room temperature with phosphate-buffered saline (PBS), centrifuged 5 min at $300 \times g$ (25ºC), resuspended in PBS and then distributed into a 96-well microplate (white Optiplate; PerkinElmer Life Sciences) at a concentration of 0.7 mg of protein/mL. This concentration allowed us to achieve luminescence levels suitable for BRET readings. Cells were then incubated for 5 min with DeepBlueC coelenterazine (PerkinElmer Life Sciences) which was manually added into each well to a final concentration of 5 μM before the addition of different ligands at increasing concentrations as indicated. BRET2 readings were taken 5 min after ligand introduction. The BRET2 signal generated by each sample was determined by calculating the ratio of the light emitted by GFP (500–530 nm) over the light emitted by *R*luc (370–450 nm) (Audet et al., 2008).

MOL #93450

6. RESULTS

Agonist-induced internalization of MOP

As opposed to other MOP agonists, in most cell types, morphine was shown to induce minimal internalization of MOP (Keith et al., 1998). We first performed immunofluorescence labeling of FlagMOP in HEK FlagMOP cells submitted to various treatments (Fig. 1A-E). The micrographs are also presented using pseudo-colors to attribute each fluorescent pixel to either the cytosol (green) or the cell membrane (purple) (Fig. 1A'-E'). Under baseline conditions, the fluorescent labeling of FlagMOP was found to be located both at the plasma membrane and in the cytoplasm (Fig. 1A, A'). For these cells, the ratio of intracellular / plasma membrane fluorescent pixels is 1.02 ± 0.07 (Fig. 1F). When cells are treated with 1 µM of morphine for 30 min (Fig. 1B, B'), the ratio of intracellular / plasma membrane labeling was not significantly changed compared with the control cells (2.12 ± 0.21 vs 1.02 ± 0.07, Fig. 1F). In contrast, a 30 min treatment with 1 µM DAMGO induced a robust internalization of MOP. In the DAMGO-treated cells, the MOP-like immunostaining was found almost exclusively inside the cells, with only discrete fluorescent puncta located at the cell membrane (Fig. 1D, D'). Quantitatively, this treatment led to a 5-fold increase in the ratio of intracellular / plasma membrane pixels (5.15 ± 0.53) compared with the control cells (Fig. 1F). The inhibition of dynamin following pretreatment with 80 µM of dynasore reversed both morphine- and DAMGO-induced increase of intracellular / cell membrane labeling ratio of MOP (Fig. 1C, C',E, E', F).

MOL #93450

ERK1/2 activation

ERK1/2 kinases are well-known downstream effectors of MOP (Al-Hasani and Bruchas, 2011). As shown in Fig. 2, a 3 min treatment with either morphine (Fig. 2A) or DAMGO (Fig. 2B) induced concentration-dependent phosphorylation of ERK1/2. Pretreatment with 10 µM of CTAP, a selective MOP antagonist, confirmed that this effect was mediated by MOP activation. As shown in Fig. 3, morphine and DAMGO also induced a similar time-dependent phosphorylation of ERK1/2. For both agonists, the maximum level of phosphorylation was reached after 3 min of stimulation, with a return to baseline values 30 min after the application of the agonist.

To further characterize the signaling events involved in the MOP-induced activation of ERK1/2, we performed experiments in which the cells were pretreated with various pharmacological inhibitors. We found that the pretreatment with 80 µM of dynasore significantly inhibited the DAMGO-induced phosphorylation of ERK1/2 (Fig. 4A). Although these results were not statistically significant, a trend was observed, suggesting that the morphine-induced activation of ERK1/2 also involves dynamin. As shown in Fig. 4B, PTX (inhibitor of $G\alpha_i$) completely blocked the morphine- and DAMGO-induced phosphorylation of ERK1/2, while CTX (activator of $G\alpha_s$) had no significant effect (Fig. 4B). Finally, we performed a concentration-response evaluation of U0126 efficacy and we found that this MEK1/2 inhibitor is ineffective when used at submicromolar concentrations. Indeed, the lowest effective concentration, i.e. the lowest concentration able to inhibit the agonist-induced activation of ERK1/2, was found to be 2 µM (Fig. 4C).

MOL #93450

SPR measurements

Next, SPR was used to assess the global cellular response resulting from the stimulation of MOP with DAMGO and morphine. We first performed SPR experiments with increasing concentrations (from 1 nM to 1 µM) of the agonists. As shown in Fig. 5A, morphine induced a concentration-dependent SPR signal. The signal was characterized by a fast increase of the reflectance value followed by a slower decrease within the next few minutes. The signal reached a plateau at approximately 30 min at each concentration. As reported in Table 1, the maximal amplitude of the SPR signal of morphine peaked at 100 nM, whereas the maximal initial slope was obtained at 10 nM. Similar results were obtained when the cells were incubated with increasing concentrations of DAMGO (Fig. 5B and Table 1). For both agonists, the signal was blocked by a pretreatment with 10 µM CTOP. Note that the injection of 10 µM CTOP (represented by # symbol in Fig. 5A and B) induced a weak SPR signal, while the vehicle (represented by + symbol in Fig. 5A and B) did not induce any detectable SPR signal other than the injection peak. SPR measurements on HEK-Mock cells, i.e., cells transfected with an empty construct, were also performed to eliminate a possible off-target effect of both MOP agonists. As expected, neither 100 nM of morphine nor DAMGO produced a detectable response (results not shown).

Pharmacological inhibitors were used to evaluate the contribution of different signaling pathways in the generation of the SPR signals induced by morphine and DAMGO. First, we investigated the implication of MOP internalization using dynasore. Because the pretreatment was conducted outside of the SPR system, we validated that dynasore had no effect on the integrity of the cell monolayer nor on the cellular membrane by

analyzing the SPR angular scans with or without pretreatment. This analysis revealed that dynasore had no effect on the SPR resonance angle ($72.97 \pm 0.07°$ vs $72.83 \pm 0.07°$, with and without pretreatment respectively; $p > 0.05$, unpaired t-test), suggesting that it did not affect the integrity of the cells. As shown in Fig. 6 and reported in Table 2, the pretreatment with dynasore produced a limited but significant decrease in the SPR signal amplitude following morphine and DAMGO treatments. Conversely, the maximal initial slope was not affected by this inhibitor (Table 2). Second, we studied the implication of G proteins using CTX and PTX. We observed that in the presence of PTX, morphine and DAMGO failed at producing any SPR signal (Fig. 7A, B). Interestingly, although CTX had no effect on the morphine- and DAMGO-induced phosphorylation of ERK1/2 (*cf.* Fig. 4A), it induced a significant decrease in the amplitude of the SPR signals induced by morphine and DAMGO (Fig. 7A, B; Table 2). Additionally, CTX had a significant effect on the maximal initial slope of the SPR response of morphine but not DAMGO (Table 2). Note that pretreatments with the toxins are not shown on their respective SPR traces because they were done 20 h before the experiments and were therefore conducted outside of the SPR chamber. As shown in Fig. 7C and 7D, the MEK1/2 inhibitor U0126, which had no effect by itself on the SPR signal other than an injection peak (# symbol), also significantly altered the amplitude of the SPR signal induced both by morphine and DAMGO, and the maximal initial slopes of both SPR responses were not significantly different (Table 2).

As mentioned above, an SPR signal profile, different from what is usually observed with vehicle, was detected following the addition of CTOP to the cells (see Fig. 5A, B). To further characterize this unexpected antagonist-induced SPR response, we extended our

study by evaluating CTOP and 3 other MOP antagonists: naltrexone, naloxone, and CTAP. As shown in Fig. 8A-D, all 4 antagonists generated notable SPR responses when used at a concentration of 10 µM on the HEK FlagMOP cells. Despite the fact that the amplitudes of the SPR signals induced by the antagonists are less important than those triggered by morphine and DAMGO, the SPR signal profiles for naltrexone, naloxone, and CTOP were very similar (compare Fig. 8A, B, and D with Fig. 5). The signal produced by CTAP is markedly different (Fig. 8C) when compared with the other antagonists. As opposed to other conditions tested in this study, CTAP led to a decrease in the reflectance value. To determine if the signals generated by the antagonists were $G\alpha_{i/o}$-mediated, we repeated these experiments in cells pre-incubated with PTX and found that the SPR responses triggered by all antagonists were abolished by PTX (Fig. 8A-D). As shown in Fig. 8E, phase-contrast microscopy revealed that the stimulation with 10 µM naltrexone induced a spreading of the cells on the surface, correlating the increase of the reflectance observed in the SPR signal. This is exemplified by a decrease of the intercellular spaces (Fig. 8E; white arrows). Conversely, stimulation with 10 µM CTAP had the opposite effect. CTAP induced a contraction of the cells accompanied by an enlargement of the intercellular spaces (Fig. 8F; white arrows), which correlates with a decrease in the reflectance observed in the SPR signal. The absence of potential off-target effects of the antagonists was confirmed by SPR measurements on HEK-Mock cells (results not shown). To assess the viability of the cells treated with PTX, we measured their ability to respond to epidermal growth factor (EGF), a tyrosine kinase receptor agonist. As shown in Fig. 10, a 20 h treatment with PTX did not significantly affect the SPR response triggered by EGF.

MOL #93450

BRET experiments

A considerable proportion of ligand-induced SPR responses were PTX sensitive, suggesting that reflectance changes by agonists and antagonists all required functional $G\alpha_{i/o}$ proteins. We had previously used BRET-based biosensors to show that occupation of delta opioid receptors by ligands of different efficacies all induced significant but distinct conformational rearrangements among heterotrimeric $G\alpha\beta\gamma$ subunits (Audet et al., 2008). Thus, it was of interest to determine whether MOP ligands which modified the basal SPR signal were also able to perturb in any way the interaction among $G\alpha\beta\gamma$ subunits. To answer this question we used BRET-based biosensors that monitor small conformational changes at the interface of the $G\alpha$ subunit and $G\beta\gamma$ dimer (Audet et al., 2008). In particular the donor was $G\alpha_{i1}$ tagged with RLuc at position 91 of the helical domain and the acceptor was $G\gamma_2$ bearing GFP at the amino-terminus (see Fig. 9B). Consistent with SPR data and with the notion that MOP ligands of different efficacies induce conformational changes among heterotrimeric subunits, DAMGO, naltrexone, and CTAP all induced concentration dependent decreases in basal energy transfer. Furthermore, BRET changes induced by the agonist DAMGO were greater than those induced by naltrexone and CTAP, which in turn did not differ from one another (Figure 9A).

7. DISCUSSION

The aim of this study was to assess downstream signaling cascades of the mu opioid receptor (MOP) in live cells using the label-free approach Surface Plasmon Resonance (SPR) spectroscopy. Our hypothesis was that different ligands acting on MOP would generate distinct SPR signatures due to the selective activation of the downstream signaling cascades. The contribution of three important components of MOP signaling (internalization of the receptor, G protein coupling, and ERK1/2 activation) was investigated on the SPR signals triggered by multiple ligands.

SPR spectroscopy is based on the quantification of discrete variations of molecular density (i.e., refractive index) within the evanescent field created at the surface of a thin gold layer on which the cells are cultured. Because the plasma membrane of cultured cells is largely confined in the evanescent field, minute changes in mass distribution (e.g. addition/retrieval of proteins) at or in the vicinity of the plasma membrane affect the integrated SPR signal (Fang et al., 2006).

In the present study, analysis of the SPR signals triggered by increasing concentrations of morphine and DAMGO revealed an initial slope that peaked at 10 nM whereas the maximal amplitude of the signal was reached at 100 nM. The reasons why the maximal slope and amplitude were not reached at the same concentrations is not clear but we hypothesize that the slope of the SPR signal represents the rate of activation of the cellular processes, likely dependent on the rate of receptor occupation, while the maximal amplitude of the signal is reached at saturating concentrations, i.e. when receptor occupation is maximal.

Because receptor internalization includes the removal of cell surface proteins and phospholipids, we expected that internalizing and non-internalizing agonists would produce distinct SPR signatures. In transfected cells, most MOP agonists but morphine are known to induce a rapid internalization of the receptor (Keith et al., 1998). In the current study, we observed that morphine elicited a limited, dynasore-sensitive increase in the intracellular/cell membrane pixels ratio over control. We also confirmed that DAMGO induced a robust internalization of MOP. Surprisingly, the SPR analyses failed to reveal any difference between the signals triggered by morphine and DAMGO. It is likely that the negative contribution of internalization is masked by cellular processes occurring simultaneously but contributing positively to the signal, such as an increased cell adhesion. Similar conclusions have been drawn for β2AR agonists (Fang and Ferrie, 2008). On the other hand, we observed that inhibition of dynamin affects both morphine- and DAMGO-induced ERK1/2 activation and SPR responses. Considering that DAMGO and morphine displayed different receptor internalization profiles but that their signaling properties were still inhibited to a similar extent by dynasore, our results suggest that dynamin may have an internalization-independent role in MOP-mediated signaling, as previously suggested by others (Whistler and von Zastrow, 1999). Although the precise mechanisms linking dynamin to MOP's downstream signaling cascades remain to be identified, the actin cytoskeleton and proteins interacting with dynamin are putative candidates (Ferguson and De Camilli, 2012).

In an effort to distinguish the responses triggered by morphine and DAMGO, we have also monitored the ERK1/2 signaling cascade and its contribution to the SPR signals. Our results revealed that the inhibition of ERK1/2 with U0126, a potent MEK inhibitor,

significantly reduced the maximal amplitude of the SPR responses induced by both MOP agonists. Other groups previously showed that the maximal responses triggered by morphine and DAMGO were barely affected by U0126 (Codd et al., 2011; Morse et al., 2011). Although Epic$^®$ (Morse et al., 2011) and SPR (current study) are dynamic mass redistribution optical biosensors, their detecting systems are slightly different. Therefore, the difference observed is likely due to the ability/sensitivity of the systems to detect specific cellular events.

Over the years, several GPCRs were analyzed using optical- and impedance-based biosensors (Peters et al., 2010). Among them, the $G\alpha_i$-coupled muscarinic type 2 receptor (M2R) was studied on both platforms. Interestingly, the signal produced upon the activation of M2R by an agonist is similar to the signals we observed after the activation of MOP. Here, we found that the inhibition of $G\alpha_i$ with pertussis toxin (PTX) abolished agonist-induced phosphorylation of ERK1/2, as well as the typical SPR signal. The PTX sensitivity of MOP-mediated ERK1/2 activation is not novel (Li and Chang, 1996; Belcheva et al., 1998). However, the fact that PTX totally abolished the SPR responses is puzzling. One could argue that an overnight PTX treatment of HEK cells could have affected their viability/integrity. However, we demonstrated that this was not the case because PTX failed to abolish the SPR signature induced by the activation of the epidermal growth factor receptor, confirming that $G\alpha_i$ signaling is essential to initiate the MOP-mediated signaling cascades measured by SPR.

We found that the treatment of HEK FlagMOP cells with CTX had no effect on morphine- and DAMGO-induced ERK1/2 phosphorylation. Surprisingly, CTX significantly modified the SPR signatures of both MOP agonists. CTX treatment is

known to elicit an increase in intracellular cAMP levels (Guerrant et al., 1974). cAMP binds and activates numerous proteins involved in various cellular processes, including the regulation of cell morphology. Morse and collaborators also found that a CTX treatment induces a decrease in the Epic® signals generated by some MOP agonists and suggested an implication of $G\alpha_s$ (Morse et al., 2011). Although it cannot be entirely ruled out, the direct implication of $G\alpha_s$ in generating the morphine- and DAMGO-mediated SPR signals is unlikely. Indeed, because it has been shown that label-free biosensors can reveal dual G protein signaling (Scott and Peters, 2010), any $G\alpha_s$-mediated effect would have been observed in the presence of PTX. Together, our observations suggest that the agonist-induced SPR responses are influenced by cAMP levels, possibly by affecting cell morphology.

One of the most intriguing findings of this study is the SPR responses induced by MOP antagonists. Our phase-contrast microscopy analysis revealed that these SPR signals are correlated with changes in cell morphology. Considering similarities with SPR signals induced by morphine and DAMGO, one possible interpretation is that the smaller, PTX-sensitive SPR changes induced by naltrexone, naloxone and CTOP reveal partial agonist properties rather than neutral antagonists. Indeed, previous studies in heterologous systems expressing MOPs indicate that naloxone inhibits cAMP production in a PTX-dependent manner (Fukuda et al., 1998). Moreover, our experiments assessing energy transfer at the $G\alpha$-$\beta\gamma$ interface revealed that naltrexone induced a concentration-dependent decrease in BRET (*cf*. Fig. 9A). A decrease in BRET at this interface is consistent with recent crystallographic evidence indicating that activation of the G protein by an agonist-occupied receptor is associated with displacement of the helical

domain of the Gα subunit away from the free terminal ends of Gβ and Gγ subunits (Rasmussen et al., 2011). Interestingly, the SPR signature triggered by CTAP differs from all other responses described in this study. Indeed, CTAP induced a decrease in reflectance while all other tested MOP ligands produced an increase. Based on the SPR signals, CTAP therefore behaves as an inverse MOP agonist. In support of our findings, CTAP has been previously described as an inverse agonist (Divin et al., 2009). Surprisingly, we observed no difference between the BRET responses induced by CTAP and naltrexone. We have previously observed that delta opioid receptor partial and inverse agonists could similarly modify energy transfer at one vantage point, but the overall conformational rearrangement at the Gα-βγ interface was still different when observed from other ones within the Gα subunit (Audet et al., 2008). A graphic representation of possible conformational changes imposed on the Gα-βγ interface by ligands of different efficacies is shown in Fig. 9B. The implication of $G\alpha_i$ in the signaling of CTAP is therefore most likely the consequence of the constitutive activity of MOP (Burford et al., 2000). In the presence of PTX, the constitutive activation of $G\alpha_i$ is abolished (Seifert and Wenzel-Seifert, 2002) which, by way of consequence, impairs the ability of CTAP to elicit a biological response. Accordingly, we found that the SPR response induced by CTAP was blunted in the presence of PTX. Finally, it is worth noting that a SPR response was observed with concentrations of agonists as low as 1 nM whereas no difference in the BRET signal was observed until 10 to 100-fold concentrations were used (compare Fig. 9A with Fig. 5B and Fig. 8A, C). We have previously shown that the BRET signals produced by G protein BRET biosensors following opioid stimulations reached a steady after 2 minutes (Audet et al., 2012;

MOL #93450

Richard-Lalonde et al., 2013). Since we performed the BRET2 readings 5 minutes after the addition of the ligands, which also corresponds to the maximal SPR response, SPR appears to be more sensitive in detecting signaling events occurring after ligand binding and receptor activation than BRET2 biosensor. Interestingly, our SPR results also revealed that the relation between agonist concentration and the maximal reflectance is biphasic while a monophasic response was observed in the BRET experiments. This may be explained by the fact that BRET experiments are designed to detect a single parameter, i.e conformational changes within the $G\alpha_i$ heteromer, whereas the purpose of SPR is to evaluate the integrated cell response.

Based on previous studies from our group (Cuerrier et al., 2008; Simard et al., 2013), we propose that an important contribution to the SPR signal following stimulation with MOP agonists, as well as MOP so-called antagonists, could be due to a $G\alpha_i$- and ERK1/2-dependent actin cytoskeleton rearrangement. Accordingly, our results revealed an important role of ERK1/2 and $G\alpha_i$ in the generation of the SPR signal evoked by the activation of MOP. In conclusion, our findings show that SPR spectroscopy is highly effective and sensitive in monitoring the integrated cell signaling upon stimulation of GPCRs, which could also represent a technical asset to address functional selectivity.

MOL #93450

9. AUTHORSHIP CONTRIBUTIONS

Participated in research design: Bourassa, Bagheri, Pineyro, Grandbois, and Gendron.

Conducted experiments: Bourassa and Bagheri.

Performed data analysis: Bourassa, Bagheri, Pineyro, Grandbois, and Gendron.

Wrote or contributed to the writing of the manuscript: Bourassa, Bagheri, Pineyro, Grandbois, and Gendron.

MOL #93450

10. REFERENCES

Al-Hasani R and Bruchas MR (2011) Molecular mechanisms of opioid receptor-dependent signaling and behavior. *Anesthesiology* **115**(6): 1363-1381.

Arttamangkul S, Quillinan N, Low MJ, von Zastrow M, Pintar J and Williams JT (2008) Differential activation and trafficking of micro-opioid receptors in brain slices. *Mol Pharmacol* **74**(4): 972-979.

Audet N, Charfi I, Mnie-Filali O, Amraei M, Chabot-Dore AJ, Millecamps M, Stone LS and Pineyro G (2012) Differential association of receptor-Gbetagamma complexes with beta-arrestin2 determines recycling bias and potential for tolerance of delta opioid receptor agonists. *J Neurosci* **32**(14): 4827-4840.

Audet N, Gales C, Archer-Lahlou E, Vallieres M, Schiller PW, Bouvier M and Pineyro G (2008) Bioluminescence resonance energy transfer assays reveal ligand-specific conformational changes within preformed signaling complexes containing delta-opioid receptors and heterotrimeric G proteins. *J Biol Chem* **283**(22): 15078-15088.

Belcheva MM, Vogel Z, Ignatova E, Avidor-Reiss T, Zippel R, Levy R, Young EC, Barg J and Coscia CJ (1998) Opioid modulation of extracellular signal-regulated protein kinase activity is ras-dependent and involves Gbetagamma subunits. *J Neurochem* **70**(2): 635-645.

Burford NT, Wang D and Sadee W (2000) G-protein coupling of mu-opioid receptors (OP3): elevated basal signalling activity. *Biochem J* **348 Pt 3**: 531-537.

Chabot V, Cuerrier CM, Escher E, Aimez V, Grandbois M and Charette PG (2009) Biosensing based on surface plasmon resonance and living cells. *Biosensors & bioelectronics* **24**(6): 1667-1673.

Cherny N, Ripamonti C, Pereira J, Davis C, Fallon M, McQuay H, Mercadante S, Pasternak G, Ventafridda V and Expert Working Group of the European Association of Palliative Care N (2001) Strategies to manage the adverse effects of oral morphine: an evidence-based report. *Journal of clinical oncology : official journal of the American Society of Clinical Oncology* **19**(9): 2542-2554.

Ciambrone GJ, Liu VF, Lin DC, McGuinness RP, Leung GK and Pitchford S (2004) Cellular dielectric spectroscopy: a powerful new approach to label-free cellular analysis. *Journal of biomolecular screening* **9**(6): 467-480.

Codd EE, Mabus JR, Murray BS, Zhang SP and Flores CM (2011) Dynamic mass redistribution as a means to measure and differentiate signaling via opioid and cannabinoid receptors. *Assay and drug development technologies* **9**(4): 362-372.

Cooper MA (2006) Optical biosensors: where next and how soon? *Drug Discov Today* **11**(23-24): 1061-1067.

Cuerrier CM, Chabot V, Vigneux S, Aimez V, Escher E, Gobeil F, Charette PG and Grandbois M (2008) Surface Plasmon Resonance Monitoring of Cell Monolayer Integrity: Implication of Signaling Pathways Involved in Actin-Driven Morphological Remodeling. *Cell Mol Bioeng* **1**(4): 229-239.

Cunningham BT, Li P, Schulz S, Lin B, Baird C, Gerstenmaier J, Genick C, Wang F, Fine E and Laing L (2004) Label-free assays on the BIND system. *Journal of biomolecular screening* **9**(6): 481-490.

Divin MF, Bradbury FA, Carroll FI and Traynor JR (2009) Neutral antagonist activity of naltrexone and 6beta-naltrexol in naive and opioid-dependent C6 cells expressing a mu-opioid receptor. *Br J Pharmacol* **156**(7): 1044-1053.

Fang Y and Ferrie AM (2008) Label-free optical biosensor for ligand-directed functional selectivity acting on beta(2) adrenoceptor in living cells. *FEBS Lett* **582**(5): 558-564.

Fang Y, Ferrie AM, Fontaine NH, Mauro J and Balakrishnan J (2006) Resonant waveguide grating biosensor for living cell sensing. *Biophys J* **91**(5): 1925-1940.

Ferguson SM and De Camilli P (2012) Dynamin, a membrane-remodelling GTPase. *Nat Rev Mol Cell Biol* **13**(2): 75-88.

Fukuda K, Kato S, Shoda T, Morikawa H, Mima H and Mori K (1998) Partial agonistic activity of naloxone on the opioid receptors expressed from complementary deoxyribonucleic acids in Chinese hamster ovary cells. *Anesthesia and analgesia* **87**(2): 450-455.

Gales C, Rebois RV, Hogue M, Trieu P, Breit A, Hebert TE and Bouvier M (2005) Real-time monitoring of receptor and G-protein interactions in living cells. *Nature methods* **2**(3): 177-184.

Giaever I and Keese CR (1993) A morphological biosensor for mammalian cells. *Nature* **366**(6455): 591-592.

Guerrant RL, Brunton LL, Schnaitman TC, Rebhun LI and Gilman AG (1974) Cyclic adenosine monophosphate and alteration of Chinese hamster ovary cell morphology: a rapid, sensitive in vitro assay for the enterotoxins of Vibrio cholerae and Escherichia coli. *Infection and immunity* **10**(2): 320-327.

Janecka A, Fichna J and Janecki T (2004) Opioid receptors and their ligands. *Current topics in medicinal chemistry* **4**(1): 1-17.

Keith DE, Anton B, Murray SR, Zaki PA, Chu PC, Lissin DV, Monteillet-Agius G, Stewart PL, Evans CJ and von Zastrow M (1998) mu-Opioid receptor internalization:

opiate drugs have differential effects on a conserved endocytic mechanism in vitro and in the mammalian brain. *Mol Pharmacol* **53**(3): 377-384.

Li LY and Chang KJ (1996) The stimulatory effect of opioids on mitogen-activated protein kinase in Chinese hamster ovary cells transfected to express mu-opioid receptors. *Mol Pharmacol* **50**(3): 599-602.

Maltais JS, Denault JB, Gendron L and Grandbois M (2012) Label-free monitoring of apoptosis by surface plasmon resonance detection of morphological changes. *Apoptosis : an international journal on programmed cell death* **17**(8): 916-925.

McPherson J, Rivero G, Baptist M, Llorente J, Al-Sabah S, Krasel C, Dewey WL, Bailey CP, Rosethorne EM, Charlton SJ, Henderson G and Kelly E (2010) mu-opioid receptors: correlation of agonist efficacy for signalling with ability to activate internalization. *Mol Pharmacol* **78**(4): 756-766.

Melnikova I (2010) Pain market. *Nat Rev Drug Discov* **9**(8): 589-590.

Morse M, Sun H, Tran E, Levenson R and Fang Y (2013) Label-free integrative pharmacology on-target of opioid ligands at the opioid receptor family. *BMC pharmacology & toxicology* **14**: 17.

Morse M, Tran E, Sun H, Levenson R and Fang Y (2011) Ligand-directed functional selectivity at the mu opioid receptor revealed by label-free integrative pharmacology on-target. *PLoS One* **6**(10): e25643.

Mulder AH, Wardeh G, Hogenboom F, Kazmierski W, Hruby VJ and Schoffelmeer AN (1991) Cyclic somatostatin analogues as potent antagonists at mu-, but not delta- and kappa-opioid receptors mediating presynaptic inhibition of neurotransmitter release in the brain. *Eur J Pharmacol* **205**(1): 1-6.

MOL #93450

Peters MF, Vaillancourt F, Heroux M, Valiquette M and Scott CW (2010) Comparing label-free biosensors for pharmacological screening with cell-based functional assays. *Assay and drug development technologies* **8**(2): 219-227.

Raehal KM, Schmid CL, Groer CE and Bohn LM (2011) Functional selectivity at the mu-opioid receptor: implications for understanding opioid analgesia and tolerance. *Pharmacol Rev* **63**(4): 1001-1019.

Rasmussen SG, DeVree BT, Zou Y, Kruse AC, Chung KY, Kobilka TS, Thian FS, Chae PS, Pardon E, Calinski D, Mathiesen JM, Shah ST, Lyons JA, Caffrey M, Gellman SH, Steyaert J, Skiniotis G, Weis WI, Sunahara RK and Kobilka BK (2011) Crystal structure of the beta2 adrenergic receptor-Gs protein complex. *Nature* **477**(7366): 549-555.

Richard-Lalonde M, Nagi K, Audet N, Sleno R, Amraei M, Hogue M, Balboni G, Schiller PW, Bouvier M, Hebert TE and Pineyro G (2013) Conformational dynamics of Kir3.1/Kir3.2 channel activation via delta-opioid receptors. *Mol Pharmacol* **83**(2): 416-428.

Scott CW and Peters MF (2010) Label-free whole-cell assays: expanding the scope of GPCR screening. *Drug Discov Today* **15**(17-18): 704-716.

Seifert R and Wenzel-Seifert K (2002) Constitutive activity of G-protein-coupled receptors: cause of disease and common property of wild-type receptors. *Naunyn-Schmiedeberg's archives of pharmacology* **366**(5): 381-416.

Simard E, Kovacs JJ, Miller WE, Kim J, Grandbois M and Lefkowitz RJ (2013) beta-Arrestin regulation of myosin light chain phosphorylation promotes AT1aR-mediated cell contraction and migration. *PLoS One* **8**(11): e80532.

MOL #93450

Stallaert W, Dorn JF, van der Westhuizen E, Audet M and Bouvier M (2012) Impedance responses reveal beta(2)-adrenergic receptor signaling pluridimensionality and allow classification of ligands with distinct signaling profiles. *PLoS One* **7**(1): e29420.

Urban JD, Clarke WP, von Zastrow M, Nichols DE, Kobilka B, Weinstein H, Javitch JA, Roth BL, Christopoulos A, Sexton PM, Miller KJ, Spedding M and Mailman RB (2007) Functional selectivity and classical concepts of quantitative pharmacology. *J Pharmacol Exp Ther* **320**(1): 1-13.

Whistler JL and von Zastrow M (1999) Dissociation of functional roles of dynamin in receptor-mediated endocytosis and mitogenic signal transduction. *J Biol Chem* **274**(35): 24575-24578.

Williams JT, Christie MJ and Manzoni O (2001) Cellular and synaptic adaptations mediating opioid dependence. *Physiological reviews* **81**(1): 299-343.

Zheng H, Loh HH and Law PY (2008) Beta-arrestin-dependent mu-opioid receptor-activated extracellular signal-regulated kinases (ERKs) Translocate to Nucleus in Contrast to G protein-dependent ERK activation. *Mol Pharmacol* **73**(1): 178-190.

MOL #93450

11. FOOTNOTES

b)

Presented in part at the 43rd Annual Meeting for The Society for Neuroscience; 2013 Nov 9-13; San Diego, CA:

[Bourassa P, Grandbois M, and Gendron L]. [Surface plasmon resonance as a tool to assess functional selectivity at the mu opioid receptor]. Program No. 799.06. 2013 Neuroscience Meeting Planner. San Diego, CA: Society for Neuroscience, 2013. Online.

MOL #93450

12. FIGURE LEGENDS

Figure 1. Agonist-induced internalization of MOP. A-E. Micrographs showing representative cells for the control (A), 1 µM morphine (B), 1 µM DAMGO (D) and dynasore pretreatment (C,E) conditions, respectively. A'-E'. Micrographs following analysis with our custom-built software integrated to ImageJ. Intracellular pixels are colored in green and cell membrane pixels are colored in purple. The micrographs showed that MOP is equally distributed between the intracellular compartment and the cell membrane in the baseline condition (A), whereas morphine stimulation (B) induced a slight increase of intracellular MOP. DAMGO stimulation (D) induced a robust increase of internalized MOP and the pretreatment with dynasore (C,E) blocked the internalization triggered by both agonists. F. Histogram representing intracellular / cell membrane ratios after quantification. *$p < 0.05$; ***$p < 0.001$ (one-way ANOVA followed by Bonferroni's *post hoc* test). The error bars indicate S.E.M.

Figure 2. Concentration-dependent effect on agonist-induced activation of ERK1/2.
A,B. Concentration-dependent effect of morphine (A) and DAMGO (B). Both morphine and DAMGO induced a concentration-dependent activation of ERK1/2, respectively reaching a peak at a concentration of 1 µM and 100 nM. This effect is blocked by a pretreatment with 10 µM CTAP. The results of the densitometric analysis are reported in the histograms. *$p < 0.05$ (one-way ANOVA with a Dunnett's *post hoc* test). The error bars indicate S.E.M.

33

Figure 3: Time course of agonist-induced activation of ERK1/2. A-B. Time course of morphine- (A) and DAMGO-induced (B) activation of ERK1/2. Morphine and DAMGO induced a similar time course of ERK1/2 activation with a maximum after 3 min of stimulation and the phosphorylation level of ERK1/2 back to baseline after 30 min. C. Graphic representation of time courses of both agonists. *$p < 0.05$, **$p < 0.01$ (one-way ANOVA with a Dunnett's *post hoc* test). The error bars indicate S.E.M.

Figure 4: Implication of MOP internalization and G protein coupling in agonist-induced activation of ERK1/2. A. Implication of MOP internalization in agonist-induced activation of ERK1/2. The pretreatment with dynasore partly blocked the activation of ERK1/2 by both morphine and DAMGO. B. Implication of $G\alpha_i$ and $G\alpha_s$ in morphine- and DAMGO-induced activation of ERK1/2. The pretreatment with PTX completely blocked the activation of ERK by both agonists, whereas the pretreatment with CTX had no effect. C. Concentration-response evaluation of U0126 efficacy. The pretreatment with U0126 is ineffective in the submicromolar concentrations whereas ERK1/2 phosphorylation is completely blunted when U0126 is used at 2 µM. The results of the densitometric analysis are reported in the histograms. *$p < 0.05$, **$p < 0.01$ and ***$p < 0.001$ (one-way ANOVA with a Bonferroni's *post hoc* test). The error bars indicate S.E.M.

Figure 5: Concentration-dependent effect of DAMGO and morphine on SPR responses. Representative SPR signals obtained for each concentration of DAMGO (A) and morphine (B). Both agonists induced a concentration-dependent increase of the

amplitude in the SPR responses with a maximum at 100 nM. This effect is blocked by a

pretreatment with 10 µM of CTOP. The signal amplitude and maximal slope were

quantified and the results are reported in table 1. Symbols legend. +:addition of vehicle;

#:addition of CTOP; *:addition of the agonist.

Figure 6: Implication of MOP internalization in the SPR responses of DAMGO and morphine. Representative SPR responses obtained with a pretreatment with 80 µM dynasore before stimulation with 100 nM morphine (A) or 100 nM DAMGO (B). For comparison purposes, the SPR signals generated with a concentration of 100 nM from Fig. 5 were placed in the same graph. The pretreatment with dynasore affected the maximal amplitude of the SPR signals of both agonists. Signal amplitude and maximal slope were quantified and the results are reported in table 2. Symbols legend: +: addition of vehicle; *: addition of the agonist.

Figure 7: Implication of G proteins and ERK1/2 in SPR responses of DAMGO and morphine. Representative SPR responses obtained with a pretreatment with 400 ng/mL CTX, 100 ng/mL PTX or 2 µM U0126 before 100 nM morphine (A-C) and 100 nM DAMGO (B-D) stimulations. For comparison purposes, SPR signals generated with a concentration of 100 nM from Fig. 5 were placed in the same graph. The pretreatments with CTX and U0126 affected the maximal amplitude of SPR signals of both agonists, whereas the pretreatment with PTX completely blocked the SPR responses. Signal amplitude and maximal slope were quantified and the results are reported in table 2. Symbols legend. +:addition of vehicle; #:addition of U0126; *:addition of the agonist.

35

MOL #93450

Figure 8: SPR responses induced by MOP antagonists. Representative SPR responses obtained for naltrexone (A), naloxone (B), CTAP (C) and CTOP (D) with and without pretreatment with 100 ng/mL of PTX. E,F. Phase-contrast microscopy assays performed with naltrexone and CTAP, respectively. Correlation between SPR measurements and phase-contrast microscopy assays can be made using roman numerals indicated by dark arrows in panels A and C and at the top right of panels E and F. All of these MOP antagonists generated detectable SPR signals and these signals were blocked with a pretreatment with PTX. These responses are correlated with changes in cell morphology because naltrexone induced a spreading and CTAP, a contraction. Symbols legend: +: addition of vehicle; *: addition of the antagonist.

Figure 9: BRET-monitored conformational changes at the Gα-βγ interface of Gα$_i$ by MOP antagonists. (A). Decrease in BRET signal induced by DAMGO (circle), naltrexone (triangle), and CTAP (square). Dose responses curves were compared by two-way ANOVA which indicated an effect of drug (p<0.001), an effect of concentration (p<0.001) and an interaction (p<0.001; n=5-6). Further analysis indicated that dose response curves by naltrexone and CTAP differed from DAMGO (p<0.001) but not among each other. (B) Schematic representation of the putative conformational changes induced by different ligands at the Gα-βγ interface as assessed by the Gαi1-Luc91/GFP-Gγ2 BRET biosensor. The ligand-free receptor is predominantly inactive as is the G protein. In this situation the donor BRET tag on the helical domain of Gαi1 (*R*luc,

36

represented in blue) and the acceptor tag on the *N*-terminus of Gγ2 (GFP, represented in green) are close to one another generating measurable basal energy transfer. Binding of a full agonist produces a large decrease in BRET which is consistent with a large displacement of the Gα helical domain away from the Gγ2 tag. Binding of partial agonist produces a smaller displacement. Being efficacious agonists, displacements by both ligands are expected to induce GDP-GTP nucleotide exchange, although reduced displacement of BRET tags by the partial agonist would suggest a more restricted exchange than for the full agonist. Binding of an inverse agonist also induces conformational changes that separate donor-acceptor tags at the Gα-βγ interface but this rearrangement would lock the G protein in a conformation that does not allow nucleotide exchange. The topography of Gαβγ trimer and its interaction with the receptor were represented as in *Rasmussen et al, 2011*.

Figure 10: EGF-induced SPR response. Representative SPR responses obtained after a stimulation with 25 ng/mL EGF, with or without a pretreatment with PTX. SPR response of EGF is unaffected by the pretreatment with PTX. Symbols legend: +: addition of vehicle; *: addition of EGF.

13. TABLES

Table 1. Agonist-sensitive profile of the SPR responses generated by morphine and DAMGO. Signal amplitude and initial slope were calculated for the SPR signals obtained following stimulation with increasing concentrations of morphine and DAMGO. RVU is an arbitrary unit (1 RVU = 0.001 unit of reflectance). The results are reported as the mean ± S.E.M (n= 5-6). * $p < 0.05$, ** $p < 0.01$, *** $p < 0.001$ (one-way ANOVA followed by a Bonferroni's *post hoc* test, compared with 1 nM results)

| Agonist concentration (nM)	Amplitude (RVU)		Slope (RVU/min)	
	DAMGO	Morphine	DAMGO	Morphine
1	50 ± 4	30 ± 2	41 ± 2	32 ± 2
10	99 ± 6 *	87 ± 7 ***	65 ± 4 *	62 ± 5 ***
100	137 ± 11 ***	131 ± 8 ***	58 ± 4	64 ± 4 ***
1000	118 ± 12 ***	116 ± 10 ***	54 ± 8	58 ± 6 **

Table 2. Effect of pharmacological inhibition of several pathways on the signal parameters of the SPR signatures of morphine and DAMGO. Signal amplitude and slope were calculated for the SPR signals obtained following a stimulation with 100 nM of agonist with indicated pretreatments. RVU is an arbitrary unit (1 RVU = 0.001 unit of reflectance). The results are reported as the mean $\pm$ S.E.M (n= 5-6). * p < 0.05, ** p < 0.01, *** p < 0.001 (one-way ANOVA followed by a Dunnett's *post hoc* test, compared with control results)

Pharmacological inhibitor	Amplitude (RVU)		Slope (RVU/min)	
	DAMGO	Morphine	DAMGO	Morphine
Control	137 ± 11	131 ± 8	58 ± 4	64 ± 4
Dynasore	112 ± 3 *	100 ± 4 **	66 ± 4	60 ± 5
CTX	92 ± 4 ***	70 ± 4 ***	52 ± 2	44 ± 2 **
U0126	108 ± 4 *	80 ± 5 ***	63 ± 3	50 ± 4

Figure 1
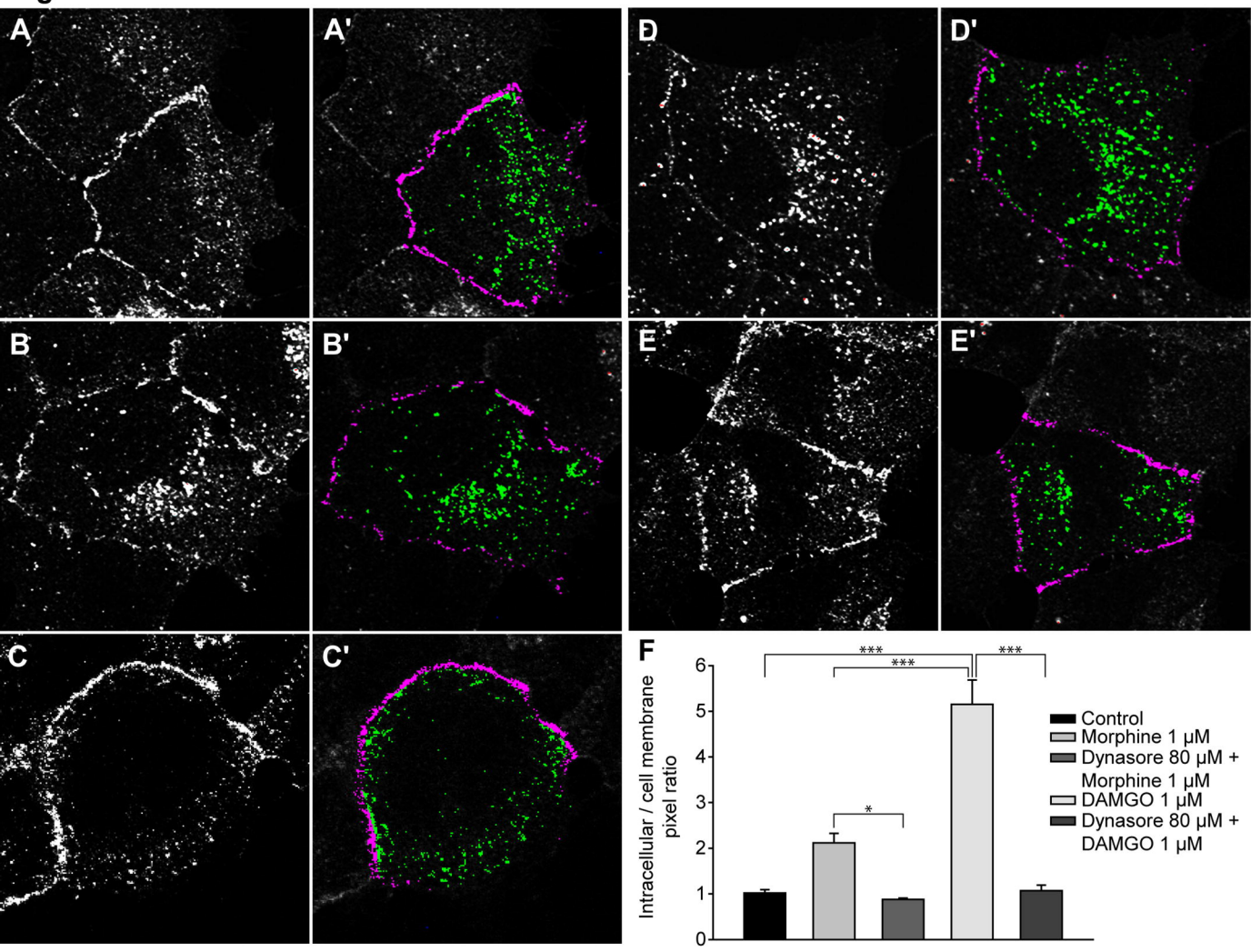
Figure 2

A
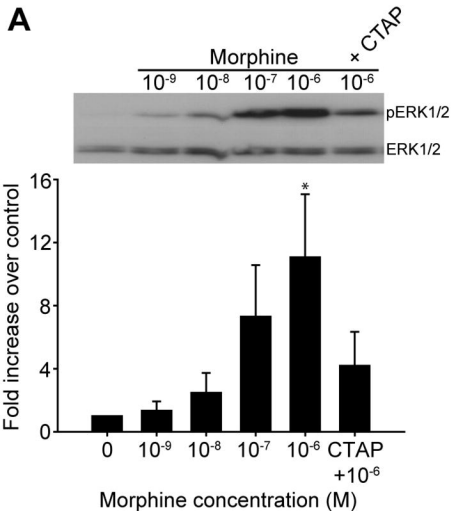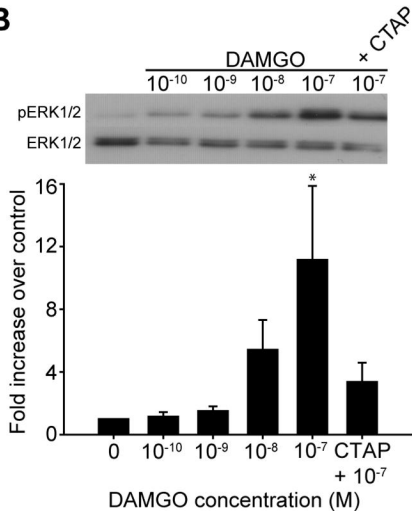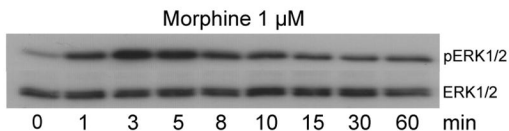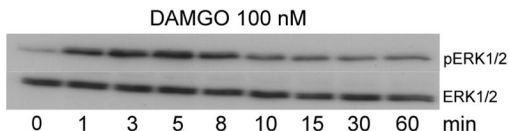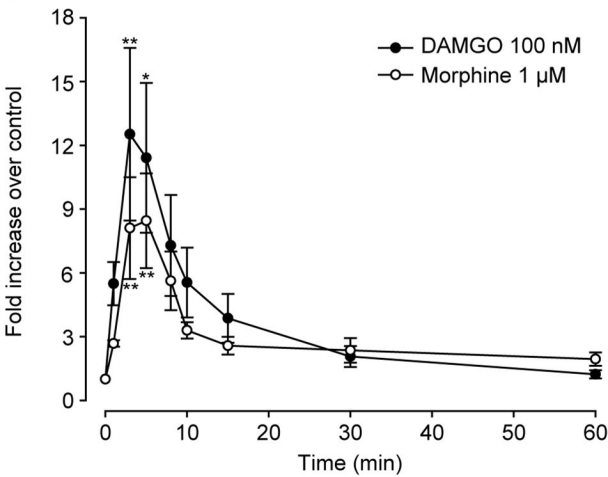
Morphine   + CTAP

10⁻⁹ 10⁻⁸ 10⁻⁷ 10⁻⁶ 10⁻⁶

pERK1/2
ERK1/2

Morphine concentration (M)

B

DAMGO   + CTAP

10⁻¹⁰ 10⁻⁹ 10⁻⁸ 10⁻⁷ 10⁻⁷

pERK1/2
ERK1/2

DAMGO concentration (M)
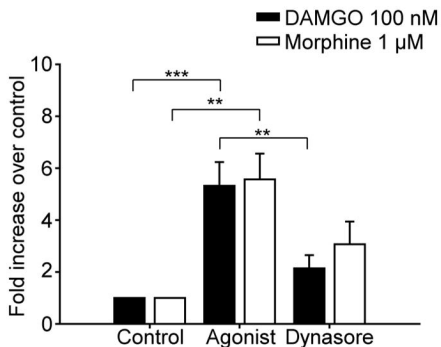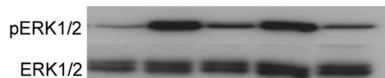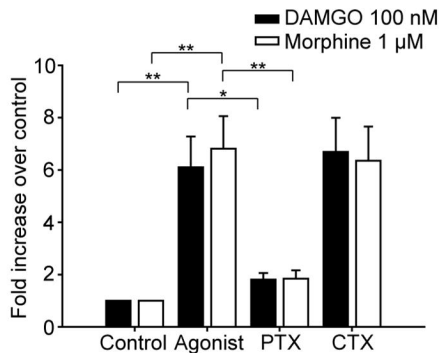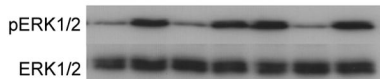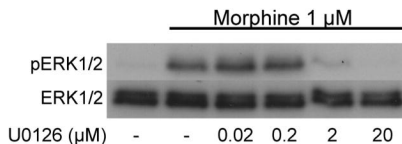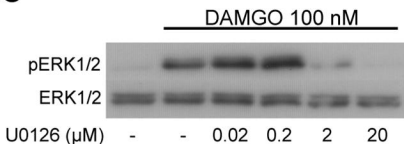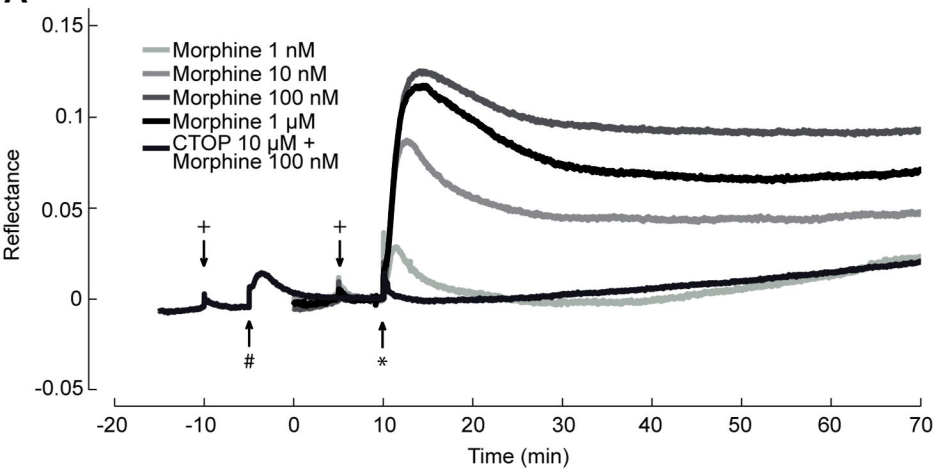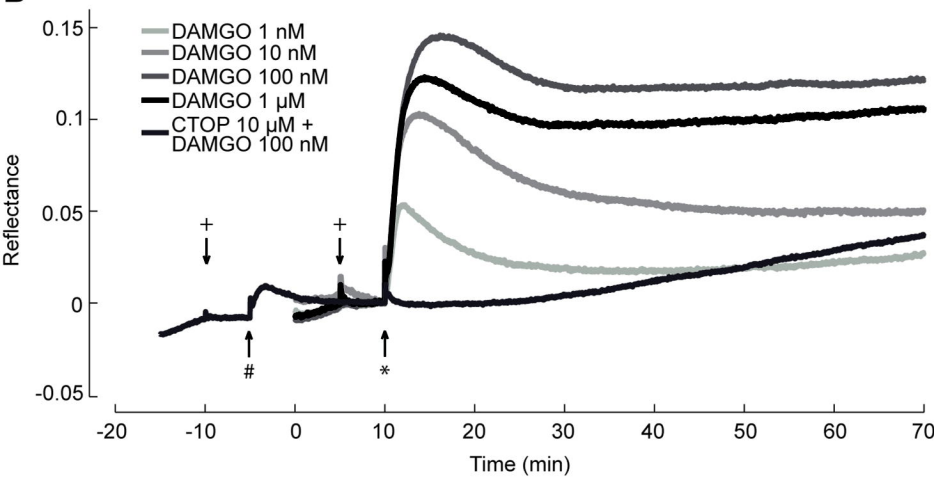
Figure 3
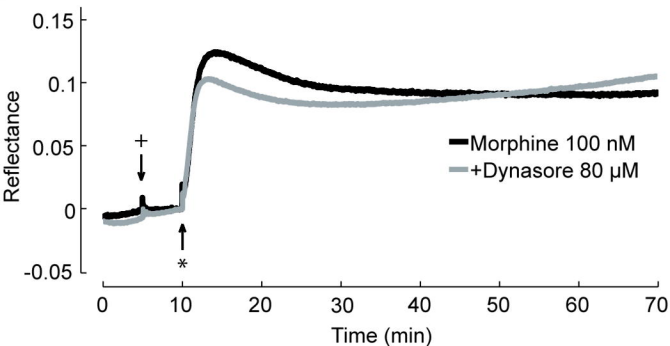
Figure 4
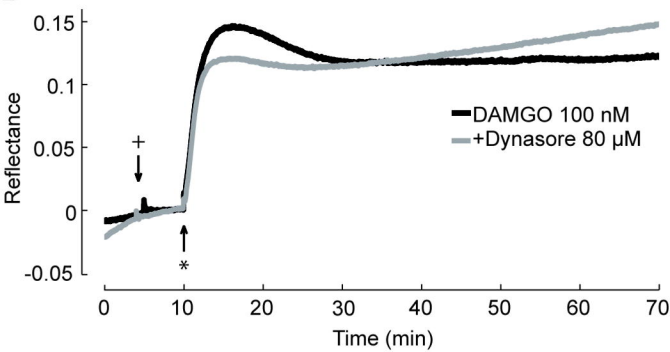
Figure 5
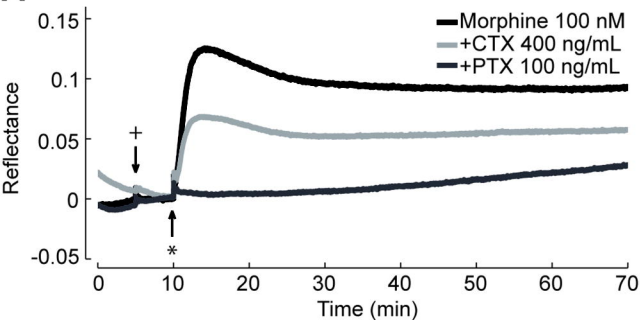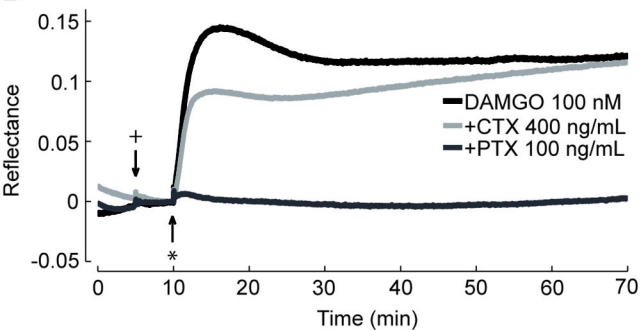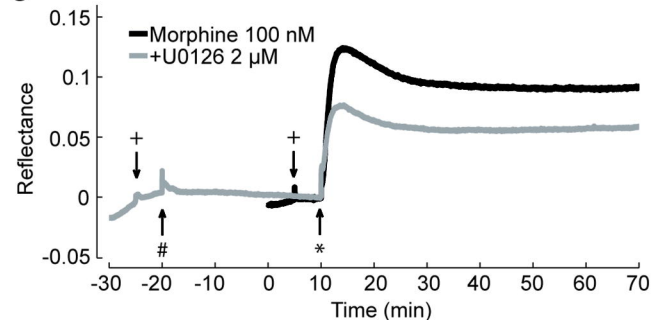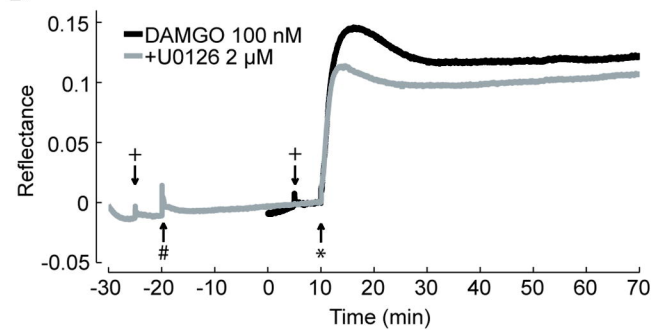
Figure 6

Figure 7

Figure 8

Figure 9

A

B

Figure 10